1

Torque Control of CSI Fed Induction Motor Drives

Aleksandar Nikolic
Electrical Engineering Institute "Nikola Tesla", Belgrade
Serbia

1. Introduction

An electric drive is an industrial system which performs the conversion of electrical energy to mechanical energy (in motoring) or vice versa (in generator braking) for running various processes such as: production plants, transportation of people or goods, home appliances, pumps, air compressors, computer disc drives, robots, music or image players etc. About 50% of electrical energy produced is used in electric drives today.
Electric drives may run at constant speed or at variable speed. Nowadays, most important are variable speed drives, especially in Europe where according to the Ecodesign for Energy-Using Products Directive (2005/32/EC) (the "EuP Directive") and its regulation regarding electric motors (Regulation 640/2009/EC) on 1 January 2015 - motors with a rated output of 7.5-375kW must meet higher energy efficiency standards, or meet the 2011 levels and be equipped with a variable speed drive.
The first motor used in variable speed applications was DC motor drive, since it is easily controllable due to the fact that commutator and stator windings are mechanically decoupled.
The cage rotor induction motor became of particular interest as it is robust, reliable and maintenance free. It has lower cost, weight and inertia compared to commutator DC motor of the same power rating. Furthermore, induction motors can work in dirty and explosive environments. However, the relative simplicity of the induction motor mechanical design is contrasted by a complex dynamic structure (multivariable, nonlinear, important quantities not observable).
In the last two decades of the 20th century, the technological improvements in power semiconductor and microprocessor technology have made possible rapid application of advanced control techniques for induction motor drive systems. Nowadays, torque control of induction motor is possible and has many advantages over DC motor control, including the same system response and even faster response in case of the latest control algorithms. Two most spread industrial control schemes employs vector or field-oriented control (FOC) and direct torque control (DTC).
Current source inverters (CSI) are still viable converter topology in high voltage high power electrical drives. Further advances in power electronics and usage of new components like SGCT (Symmetric Gate Commutated Thyristor), gives the new possibilities for this type of converter in medium voltage applications. Power regeneration during braking, what is a one of main built-in feature of CSI drives, is also merit for high power drives. Despite the

above advantages, the configuration based on a thyristor front-end rectifier presents a poor and variable overall input power factor (PF) since the current is not sinusoidal, but trapezoidal waveform. Also, the implementation of CSI drive systems with on-line control capabilities is more complex than for voltage source inverters (VSI), due to the CSI gating requirements. Regarding mentioned disadvantages, CSI drives are of interest for research in the field of torque control algorithms, such as vector control (or FOC) and direct torque control (DTC). This chapter will present basic FOC and DTC algorithms for CSI drives and show all features and disadvantages of those control schemes (sluggish response, phase error, large torque ripples, need for adaptive control, etc.). Using recent analysis tools like powerful computer simulation software and experiments on developed laboratory prototype two new FOC and DTC solutions will be presented in the chapter. The proposed FOC enables CSI drive to overcome mentioned inconveniences with better dynamic performances. This enhancement relies on fast changes of the motor current, without phase error, similar to the control of current regulated voltage source PWM inverter. The realized CSI drive has more precise control, accomplished by the implemented correction of the reference current. This correction reduces the problem of the incorrect motor current components produced by the non-sinusoidal CSI current waveform. On the other side, proposed DTC algorithm is completely new in the literature and the only such a control scheme intended for CSI induction motor drives. Presented DTC is based on the constant switching frequency, absence of coordinate transformation and speed sensor on the motor shaft. Furthermore, since flux estimator is based only on DC link measurements, there is not necessity for any sensor on the motor side which is one of main drive advantages. In this case, by combination of vector control and basic DTC, a robust algorithm is developed that has a faster torque response and it is simpler for implementation.

2. Characteristics of current source inverters

The most prevailing industrial drive configuration in low voltage range is based on IGBT transistors as power switches and voltage-source inverter (VSI) topology. On the other side, the induction motor drives with thyristor type current-source inverter (CSI, also known as auto sequentially commutated inverter, Fig. 1) possess some advantages over voltage-source inverter drive, but it has a larger torque ripples since the current wave-form is not sinusoidal. Furthermore, due to the nature of the CSI operation, the dynamic performance that exists in VSI PWM drives could not be achieved. But, CSI permits easy power regeneration to the supply network under the breaking conditions, what is favorable in large-power induction motor drives. At low voltage range (up to 1kV) this type of inverter is very rare and abandoned, but this configuration is still usable at high power high voltage range up to 10kV and several MW. In traction applications bipolar thyristor structure is replaced with gate turn-off thyristor (GTO). Nowadays, current source inverters are very popular in medium-voltage applications, where symmetric gate-commutated thyristor (SGCT) is utilized as a new switching device with advantages in PWM-CSI drives (Wu, 2006). New developments in the field of microprocessor control and application in electrical drives gives possibility for employment of very complex and powerful control algorithms. Torque control of CSI fed induction motor drives becomes also viable and promising solution, since some of CSI control disadvantages could be overcome using improved mathematical models and calculations.

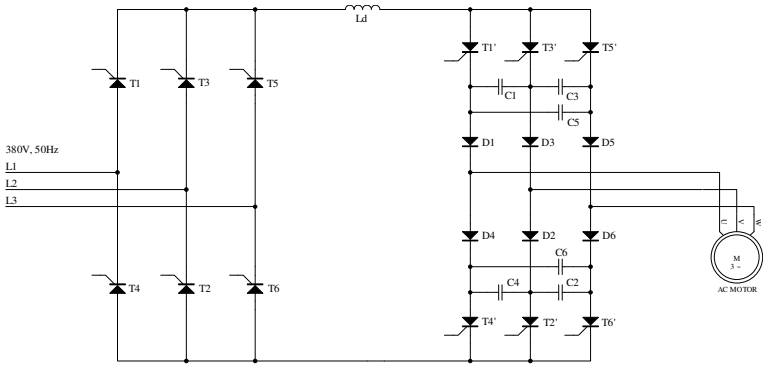

Fig. 1. Basic CSI topology using thyristors as power switches

Two most important torque control schemes are presented, namely FOC and DTC. Both control schemes will be shown with all variations known from literature, including those proposed by previous research work of author. All presented torque control algorithms, basic and proposed by author, are analyzed and verified by simulations and experiments.

3. Vector control

In the past, DC motors were used extensively in areas where variable-speed operation was required, since their flux and torque could be controlled easily by the field and armature current. However, DC motors have certain disadvantages, which are due to the existence of the commutator and brushes. On the other side, induction motors have less size for the same power level, has no brushes and commutator so they are almost maintenance free, but still has disadvantages. The control structure of an induction motor is complicated since the stator field is revolving. Further complications arise due to the fact that the rotor currents or rotor flux of a squirrel-cage induction motor cannot be directly monitored.

The mechanism of torque production in an AC and DC machine is similar. Unfortunately, that similarity was not emphasized before 1971, when the first paper on field-oriented control (FOC) for induction motors was presented (Blaschke, 1971). Since that time, the technique was completely developed and today is mature from the industrial point of view. Today field oriented controlled drives are an industrial reality and are available on the market by several producers and with different solutions and performance.

3.1 Basic vector control of CSI drives

Many strategies have been proposed for controlling the motion of CSI fed induction motor drives (Bose, 1986; Novotny & Lipo, 1988; Wu et al., 1988; Deng & Lipo, 1990; Vas, 1990). The vector control has emerged as one of the most effective techniques in designing high-performance CSI fed induction motor drives. Compared to the PWM VSI drives CSI has advantage in the reversible drives, but it has a larger torque ripples since the current wave-form is not sinusoidal. Furthermore, due to the nature of the CSI operation, the dynamic performance that exists in PWM drives are not achieved with the existing vector control algorithms.

The well-known ("basic") structure of a CSI fed induction motor drive with indirect vector control is shown in Fig. 2 (Bose, 1986; Vas, 1990).

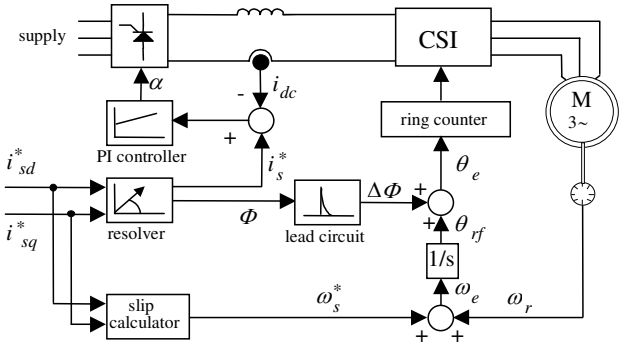

Fig. 2. Indirect vector control of a CSI fed induction machine

This method makes use of the fact that satisfying the slip relation is a necessary and sufficient condition to produce field orientation, i.e. if the slip relation is satisfied (denoted as slip calculator in Fig. 2), current *d* component will be aligned with the rotor flux. Current commands are converted to amplitude and phase commands using resolver (rectangular to polar coordinate transformation). The current amplitude command is directly employed as the reference for the current PI controller intended for controlling the input converter (three phase full wave bridge rectifier). The phase command is passed through a lead circuit such that phase changes are added into the inverter frequency channel, since these instantaneous phase changes are not contained in the slip frequency command signal coming from the slip calculator.

3.2 Proposed vector control of CSI drives

In the vector controlled CSI drives found in (Bose, 1986; Wu et al., 1988; Deng & Lipo, 1990; Vas, 1990; Novotny & Lipo, 1996) and shown in previous chapter, the problems of the speed response are reported. This is influenced by the instantaneous phase error and, as a result, these configurations have slower torque response compared to the current regulated PWM drives. In addition to the phase error, the commutation delay and the non-sinusoidal supply that is inhered in CSI operation must be generally compensated for, to achieve acceptable vector control. To overcome these disadvantages the phase error elimination and the reference current correction should be performed.

In this chapter, the vector control algorithm that eliminates the two drawbacks is shown (Nikolic & Jeftenic, 2006). The suggested algorithm produces the performance of the CSI drive that exists in the PWM vector controlled drives. That enables this simple and robust configuration to be used in applications where reversible operation is a merit.

The necessity for the phase error elimination can be explained with the help of the following phasor diagram:

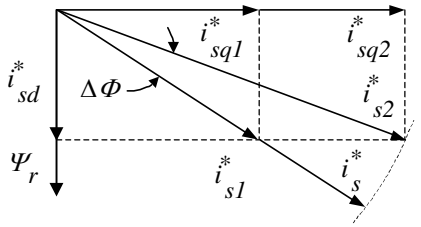

Fig. 3. Phasor diagram with shown phase error

When the torque command is stepped from i_{sq1}* to i_{sq2}* (with a constant i_{sd}*), the current vector should instantaneously change from i_{s1}* to i_{s2}*. The slip frequency should also change immediately. The resolver does give the correct amplitude and the new slip frequency will be obtained by the slip calculator. However, although the phase change $\Delta\Phi$ is added by a lead circuit as shown in Fig. 2, since the instant phase changes are not contained in the slip frequency command signal coming from the slip calculator (Bose, 1986; Deng & Lipo, 1990; Novotny & Lipo, 1996), the stator current command will correspond to the vector i_s* in Fig. 3, and there will be a phase error in the vector control system. This would result in an instantaneous loss of the field-orientation that produces a very sluggish response of both flux and torque. This problem could be overcome by the proposed algorithm, which unifies features of both PWM and CSI converter. The resolver is still used to calculate the rectifier reference current, but for the inverter thyristors control, a method used in the current controlled PWM inverter is implemented. Instead of a lead circuit (shown in Fig. 2), the new algorithm includes a synchronous to stator transformation (T^{-1}) to transfer the d-q commands to the three-phase system. This is essential for achieving a fast torque response, since the torque value is determined by the fundamental harmonic of the stator current.

For correct firing of the thyristors in the inverter, the switching times should be properly determined to ensure that the phase angle of the motor current matches the phase angle of the reference currents in a-b-c system. The reference sinusoidal currents obtained as a result of transformation T^{-1} are divided by the value obtained on the resolver output to produce currents of unity amplitudes. Introduction of these currents into the comparator with trigger level equal to 0.5 gives the proper thyristor conduction time of 120 degrees. This is illustrated in Fig. 4, where i_a* is unity sinusoidal current, i_a is scaled CSI output current and i_{a1} is fundamental stator current.

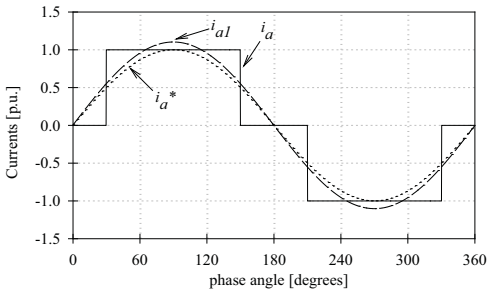

Fig. 4. Waveforms of the reference current and fundamental stator current

The algorithm possesses the additional advantage regarding the practical realization. In digital control system the lead circuit divides the difference of the two succeeding samples with the sampling time. Since the sampling time is small, this operation produces the computational error. The phasor diagram from Fig. 3 with removed phase error is presented in Fig. 5.

Without the phase error ($\Delta\Phi = 0$), the step of the torque command produces the new stator current command (i_s* = i_{s2}*). Due to non-sinusoidal currents of the CSI, the average values of the motor d-q currents i_{sd_av} and i_{sq_av} and the resulting stator current vector is greater than the corresponding references shown in Fig. 5. To improve proposed algorithm and avoid improper resultant d-q motor currents, the rectifier reference current correction is performed.

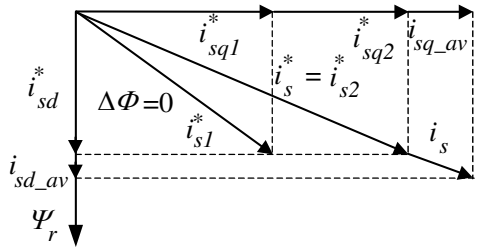

Fig. 5. Phasor diagram without phase error

In the vector controlled induction motor drive fed by a CSI a problem of incorrect copying of the d-q references to the motor exist. As stated earlier, the reason is non-sinusoidal current waveform produced by a CSI. The ideal CSI current is a quasi-square waveform (shown in Fig. 4). The Fourier analysis of this waveform gives the expression:

$$i_a = \frac{2\sqrt{3}}{\pi} \cdot I_d \cdot \left(\sin(\omega t) - \frac{1}{5}\sin(5\omega t) - \frac{1}{7}\sin(7\omega t) + \cdots \right) \tag{1}$$

The previous relation shows that the fundamental component of AC output current has the amplitude 10 percent greater than the value of DC link current. For correct reproduction of the d-q references and satisfactory vector control it is not sufficient to adjust only the phase of the fundamental motor current and the phase angle of the generated commands. The fine-tuning of the motor currents in d-q frame is required.

To avoid supplementary hardware and software, a procedure that relies only on the values calculated off-line is proposed. The corresponding relation between the mean values of the motor currents in d-q frame and the commanded d-q currents is calculated. For proposed correction it is not sufficient to use the difference between currents of 10% from (1), because the correction depends on the phase angle of the d-q components and the inverter commutation process. At lower speed, the commutation process could be neglected since it is much shorter than the motor current cycle. Taking all this in consideration, the rectifier reference current is corrected concerning the reference amplitude, the phase angle and the commutation duration. The rectifier reference current formed in that manner is now introduced to the current controller to obtain suitable motor d-q currents and achieve desired vector control.

The calculation starts from the fundamental reference current from the resolver:

$$i^*_s = \sqrt{(i^*_{sd})^2 + (i^*_{sq})^2} \tag{2}$$

and the phase angle (also obtained from the resolver):

$$\Phi = \arctan\left(i^*_{sd} / i^*_{sq}\right) \tag{3}$$

Since the inverter commutation process is not neglected, the waveform of the inverter output current is represented by a trapezoidal approximation analyzed in (Cavalini et al., 1994) with adequate precision. Trapezoidal waveform is very near to the real current cosine waveform due to the short commutation period, as explained in (Bose, 1986). This approximation assumes that during the commutation period the inverter current rises with

a constant rate of change. For rated rectifier current I_d the current rate of change during the commutation is equal to I_d/t_c, where t_c is corresponding commutation time calculated from the values of the commutation circuit components. The adequate commutation angle μ could be obtained as a product of the inverter frequency ω_e and particular commutation time. This time interval is determined from the current rate of change I_d/t_c and the reference value of the DC link current i_s*, therefore the commutation angle is:

$$\mu = \omega_e \cdot \frac{t_c}{I_d} \cdot i_s^* \tag{4}$$

Since the inverter current is periodical, the trapezoidal waveform in all three phases could be represented on a shorter angle interval with the following equations:

$$i_a(\theta,\mu,\Phi) = \begin{cases} 0 & \theta < \Phi - \frac{\pi}{3} \\ \frac{I_d}{\mu} \cdot \left(\theta - \Phi + \frac{\pi}{3}\right) & \theta < \Phi - \frac{\pi}{3} + \mu \\ I_d & \theta < \Phi + \frac{\pi}{3} \\ I_d - \frac{I_d}{\mu} \cdot \left(\theta - \Phi - \frac{\pi}{3}\right) & \theta < \Phi + \frac{\pi}{3} + \mu \\ 0 & \theta < \pi \end{cases} \tag{5}$$

$$i_b(\theta,\mu,\Phi) = i_a(\theta - \frac{2\pi}{3},\mu,\Phi) \tag{6}$$

$$i_c(\theta,\mu,\Phi) = i_a(\theta - \frac{4\pi}{3},\mu,\Phi) \tag{7}$$

where θ ranges from 0 to π, μ is the commutation angle and Φ is the phase angle obtained from (3). The instantaneous values of d-q currents are solved by a three phase to d-q frame transformation T:

$$\begin{bmatrix} i_{sd}(\theta,\mu,\Phi) \\ i_{sq}(\theta,\mu,\Phi) \end{bmatrix} = \frac{2}{3} \cdot \mathbf{T} \cdot \begin{bmatrix} i_a(\theta,\mu,\Phi) \\ i_b(\theta,\mu,\Phi) \\ i_c(\theta,\mu,\Phi) \end{bmatrix} = \\ = \frac{2}{3} \cdot \begin{bmatrix} \sin(\theta) & \sin(\theta - 2\pi/3) & \sin(\theta - 4\pi/3) \\ \cos(\theta) & \cos(\theta - 2\pi/3) & \cos(\theta - 4\pi/3) \end{bmatrix} \cdot \begin{bmatrix} i_a(\theta,\mu,\Phi) \\ i_b(\theta,\mu,\Phi) \\ i_c(\theta,\mu,\Phi) \end{bmatrix} \tag{8}$$

The average values of the currents in d and q axis obtained from (8) on the range from 0 to π be:

$$i_{sd\_av}(\mu,\Phi) = \frac{1}{\pi} \cdot \int_0^{\pi} i_{sd}(\theta,\mu,\Phi)\,\mathrm{d}\,\theta \tag{9}$$

$$i_{sq\_av}(\mu,\Phi)=\frac{1}{\pi}\cdot\int_0^{\pi} i_{sq}(\theta,\mu,\Phi)\,\mathrm{d}\,\theta \tag{10}$$

The amplitude of the motor current vector in polar coordinates could be determined using the average values obtained from (9) and (10):

$$i_s(\mu,\Phi)=\sqrt{i_{sd\_av}^2(\mu,\Phi)+i_{sq\_av}^2(\mu,\Phi)} \tag{11}$$

The difference between reference amplitude calculated from (2) and the resulting stator amplitude obtained from (11) is shown in Fig. 4. To avoid this difference, the corresponding correction factor f_{cor} is introduced as a ratio of the reference (2) and the actual motor current (11):

$$f_{cor}(\mu,\Phi)=\frac{i_s^*}{i_s(\mu,\Phi)} \tag{12}$$

For simulation and practical realization purposes, the correction factor f_{cor} is computed from (2) – (12), and placed in a look-up table with the following restrictions:

- i_{sd}* is constant,
- i_{sq}* is changed only to its rated value with i_s* limited to 1 p.u.
- for given references, all possible values of Φ and μ are calculated using (3) and (4), respectively.

The rectifier reference current that provides the correct values of motor current d-q components is now:

$$i_{ref}=i_s^*\cdot f_{cor}(\mu,\Phi) \tag{13}$$

The interdependence between correction factor f_{cor}, commutation angle μ and phase angle Φ is presented in Fig. 6 as a 3-D graph.

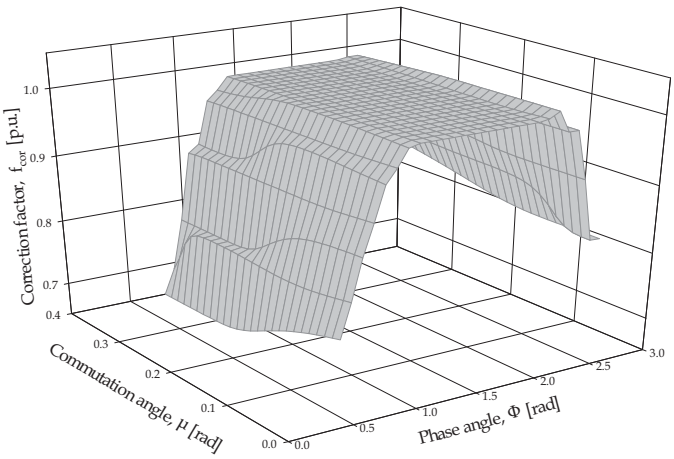

Fig. 6. Correction factor, commutation angle and phase angle interdependence

The calculated results of the current correction in d-axis and q-axis are presented in Fig. 7a and Fig. 7b respectively. The corrected currents are given along with references and motor average d-q currents (values without correction). The flux command is held constant (0.7 p.u.), while torque command is changed from –0.7 p.u. to 0.7 p.u.

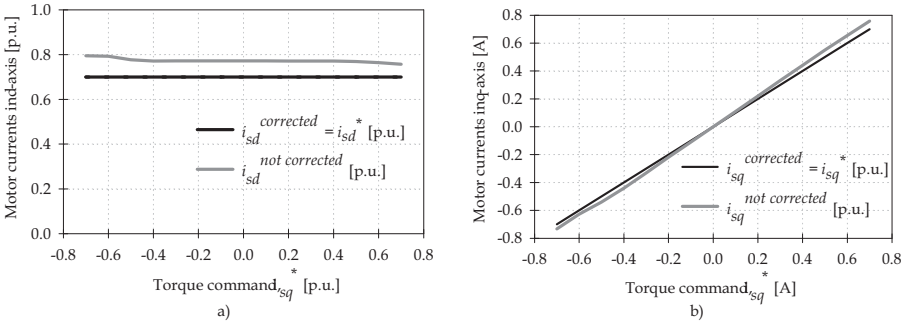

Fig. 7. Calculated motor current corrected in d-axis and q-axis (a,b respectively)

From the previous analysis the new resolver with current correction is formed as shown in Fig. 8. This structure is used both in the simulations and the experiments. The new resolver is consisted of the block "Cartesian to polar" (the coordinate transformation) and the block "Correction" that designates the interdependence given in Fig. 6. As stated before, this interdependence is placed in a 3-D look-up table using (2)-(12).

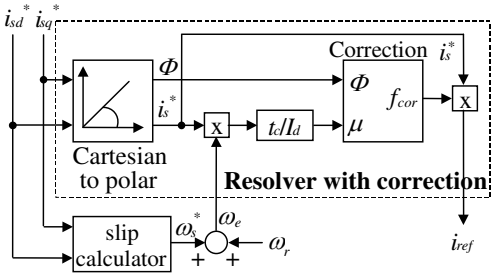

Fig. 8. New resolver with current correction

To analyze dynamic performances of the proposed CSI drive, the torque response of the "basic" structure shown in Fig. 2 is compared to the response of the new vector control algorithm. This is done by simulations of these two configurations' mathematical models in Matlab/Simulink. The first model represents the drive with basic arrangement and the second is the drive with new control algorithm. The simulation of both models is done with several initial conditions. Magnetizing (d-axis) current for rated flux has been determined from the motor parameters and its value (0.7p.u.) is constant during simulations. The rated q-axis current has been determined from the magnetizing current and the rated full-load current using (2). At first, simulations of both models are started with d-axis command set to 0.7p.u, no-load and all initial conditions equal to zero. When the rotor flux in d-axis approaches to the steady state, the machine is excited. This value of d-axis flux is now initial

for the subsequent simulations. For the second simulation the pulse is given as a torque command, with the amplitude of 0.2p.u. and duration of 0.5s. With no-load, the motor will be accelerated from zero speed to the new steady-state speed (0.2p.u.), which is the initial condition for the next simulation. Finally, the square wave torque command is applied to both models with equal positive and negative amplitudes (±0.2p.u) and the observed dynamic torque response is extracted from the slope of the speed (Lorenz, 1986). The square wave duty cycle (0.9s) is considerably greater than the rotor time constant (T_r = 0.1s), hence the rotor flux could be considered constant when the torque command is changed. Fig. 9 shows torque, speed and rotor flux responses of both models. It could be noticed that the torque response of the basic structure is slightly slower (Fig. 9a), while the proposed algorithm gives almost instantaneous torque response (Fig. 9b). This statement could be verified clearly from the speed response analysis. In both cases the torque command is the same. In the new model this square wave torque command produces speed variations from 0.2p.u. to 0.6p.u. with identical slope of the speed. But, in the basic model at the end of the first cycle the speed could not reach 0.6p.u. for the same torque command due to the fact

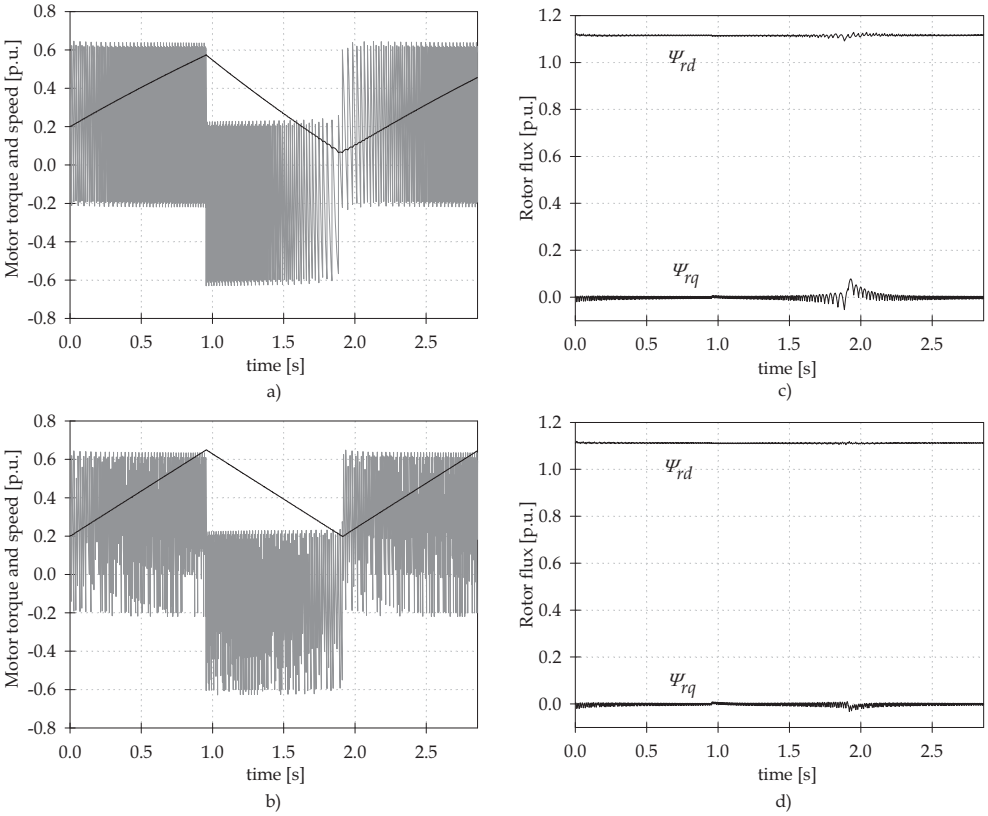

Fig. 9. Torque, speed and rotor flux of the basic structure (a), (c) and of the proposed algorithm (b), (d)

that torque response is slower. Also, in the next cycle (negative torque command) the speed does not return to 0.2p.u. for the same reason. From different slopes of the speed in these two models it could be concluded that proposed algorithm produces quicker torque response. The rotor q-axis flux disturbance in transient regime that exists in the basic model (Fig. 9c) is greatly reduced by the proposed algorithm in the new model (Fig. 9d). It could be seen that some disturbances also exist in the case of d-axis flux, but they are almost disappeared in the new model.

To illustrate the significance and facilitate the understanding of theoretical results obtained in the previous section, a prototype of the drive is constructed. The prototype has a standard thyristor type frequency converter digitally controled via Intel's 16-bit 80C196KC20 microcontroller. Induction motor used in laboratory is 4kW, 380V, 50Hz machine. The speed control of the drive and a prototype photo are shown in Fig. 10. Simplicity of this block diagram confirms that the realized control algorithm is easier for a practical actualization.

The proposed circuit for the phase error elimination is at first tested on the simulation model. The simulation is performed in such a manner that C code for a microcontroller could be directly written from the model. The values that are read from look-up tables in a real system (cosine function, square root) are also presented in the model as tables to properly emulate calculation in the microcontroller.

Fig. 11a shows waveforms of the unity sinusoidal references (i_a* and i_b*) while Fig. 11b indicates inverter thyristors switching times with changed switching sequence when the phase is changed (0.18s, marked with an arrow). On these diagrams it could be observed that thyristors T_1 and T_2 are switched to ON state when unity references i_a* and i_b* reach 0.5 p.u., respectively. Fig. 11c,d represents the instant phase variation of the currents in *a* and *b* phases after the reference current is altered. The corresponding currents without command changes are displayed with a thin line for a clear observation of the instant when the phase is changed.

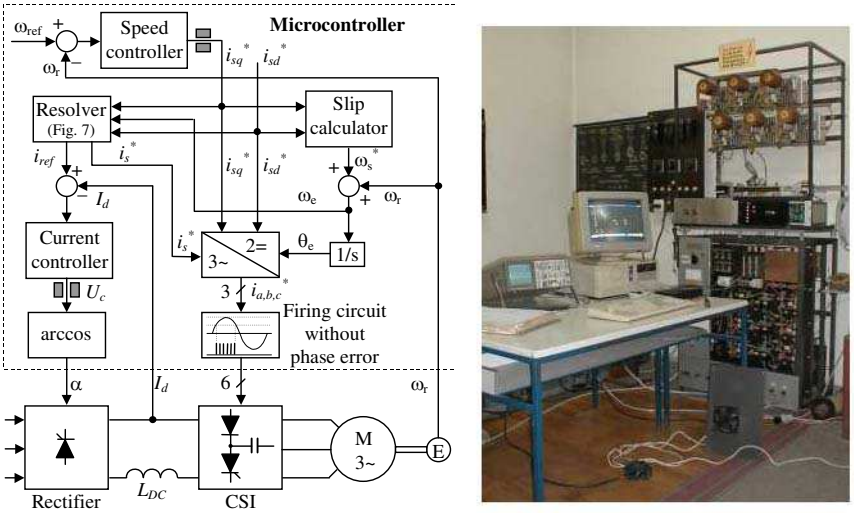

Fig. 10. CSI fed induction motor drive with improved vector control algorithm: control block diagram (left), laboratory prototype (right)

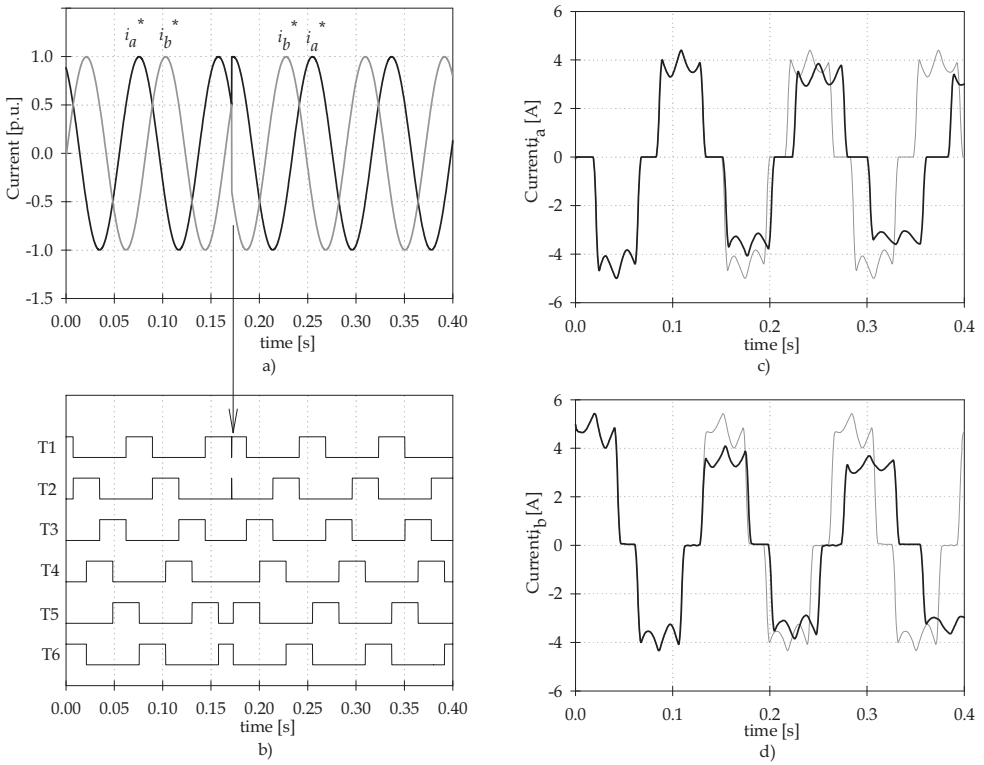

Fig. 11. Results of the phase error elimination (a,b - simulation, c,d - experimental)

The effects of the reference current correction are given by the specific experiment. To estimate d and q components, the motor currents in *a* and *b* phases and the angle θ_e between *a*-axis and *d*-axis are measured. This angle is obtained in the control algorithm (Fig. 10) as a result of a digital integration:

$$\theta_e(n) = \theta_e(n-1) + \omega_e \cdot T_s \tag{14}$$

where n is a sample, T_s is the sample time and ω_e is excitation frequency. The integrator is reset every time when θ_e reaches 0 or 360 degrees. The easiest way for acquiring the value of this angle is to change the state of the one microcontroller's digital output at the instants when the integrator is reset. On the time range between two succeeding pulses the angle is changed linearly from 0 to 360 degrees (for one rotating direction). Since only this time range is needed for determine the currents in d and q axis, the reset signal from the digital output is processed to the external synchronization input of the oscilloscope. In that way the motor phase currents are measured only on the particular time (angle) range. The corresponding currents in d-q axes are calculated from (8) using for θ_e, i_a and i_b experimentally determined values.

The experimental results are given in Fig. 12 with disabled speed controller.

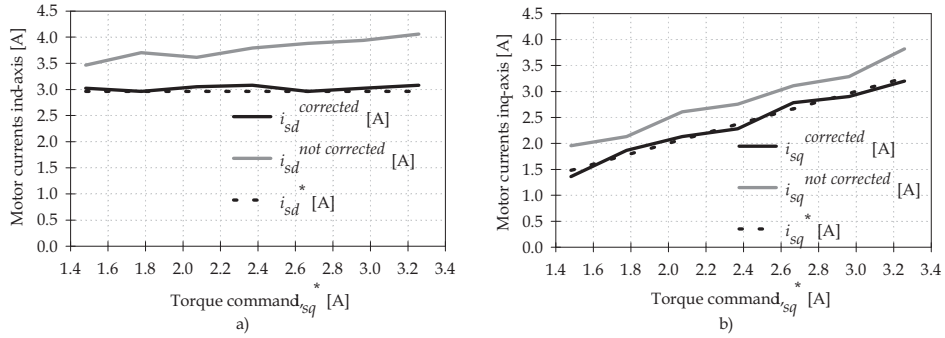

Fig. 12. Experimental results of the motor current correction in d-axis and q-axis (a,b respectively)

The flux reference was maintained constant at 2.96A (0.7p.u.) and torque command was changed from 1.5A (0.35p.u.) to 3.3A (0.78 p.u.). The inverter output frequency is retained the same during experiment (≈20Hz) by varying the DC motor armature current. From Fig. 12 it could be seen that for the proposed algorithm average values of d-q components in the p.u. system are almost equal to corresponding references. On the other side, in the system without correction there is a difference up to 15%, which confirmed the results obtained from calculations shown in Fig. 7. This difference produces steady state error, what makes such a system unacceptable for vector control in high performance applications.
On the Fig. 13 the motor speed and rotating direction changes are shown with enabled speed controller. The reference speed is swapped from -200min^{-1} to +200min^{-1}.

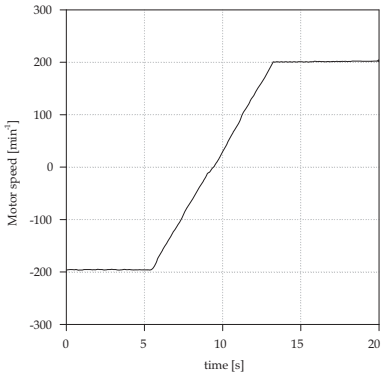

Fig. 13. The motor speed reversal

In Fig. 14 the influence of the load changes to the speed controller is presented. As a load, DC machine (6kW, 230VDC, controlled by a direct change of the armature current via 3-phase rectifier) is used. At first, the induction motor works unloaded in a motor region (M) with the reference speed of –200min^{-1} that produces the torque command current i_{sq1}^* = -1.57A. After that, the DC machine is started with its torque in the same direction with rotating direction of the induction motor. That starts the breaking of the induction motor and it goes to the generator region (G). In this operating region the power from DC link

returns to the supply network. The reference torque command current changes its value and sign (i_{sq2}* = 1.72A). When DC machine is switched off, the induction motor goes to the motor region (M) and the reference torque command current is now i_{sq3}* = -1.48A.

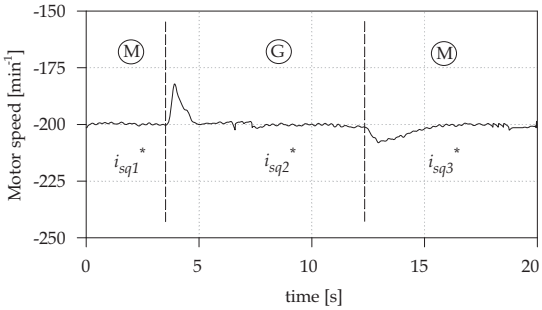

Fig. 14. The load changes at motor speed of –200min^{-1}

4. Direct torque control

The direct torque control (DTC) is one of the actively researched control schemes of induction machines, which is based on the decoupled control of flux and torque. DTC provides a very quick and precise torque response without the complex field-orientation block and the inner current regulation loop (Takahashi & Noguchi, 1986; Depenbrok, 1988). DTC is the latest AC motor control method (Tiitinen et al., 1995), developed with the goal of combining the implementation of the V/f-based induction motor drives with the performance of those based on vector control. It is not intended to vary amplitude and frequency of voltage supply or to emulate a DC motor, but to exploit the flux and torque producing capabilities of an induction motor when fed by an inverter (Buja et al., 1998).

4.1 Direct torque control concepts

In its early stage of development, direct torque control is developed mainly for voltage source inverters (Takahashi & Noguchi, 1986; Tiitinen et al., 1995; Buja, 1998). Voltage space vector that should be applied to the motor is chosen according to the output of hysteresis controllers that uses difference between flux and torque references and their estimates. Depending on the way of selecting voltage vector, the flux trajectory could be a circle (Takahashi & Noguchi, 1986) or a hexagon (Depenbrok, 1988) and that strategy, known as Direct Self Control (DSC), is mostly used in high-power drives where switching frequency is need to be reduced.

Controllers based on direct torque control do not require a complex coordinate transform. The decoupling of the nonlinear AC motor structure is obtained by the use of on/off control, which can be related to the on/off operation of the inverter power switches. Similarly to direct vector control, the flux and the torque are either measured or mostly estimated and used as feedback signals for the controller. However, as opposed to vector control, the states of the power switches are determined directly by the estimated and the reference torque and flux signals. This is achieved by means of a switching table, the inputs of which are the

torque error, the stator flux error and the stator flux angle quantized into six sections of 60°. The outputs of the switching table are the settings for the switching devices of the inverter. The error signal of the stator flux is quantized into two levels by means of a hysteresis comparator. The error signal of the torque is quantized into three levels by means of a three stage hysteresis comparator (Fig. 15).

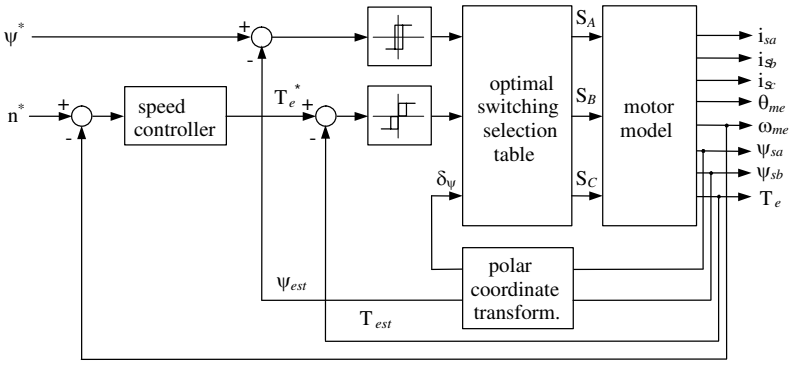

Fig. 15. Basic concept of direct torque control

The equation for the developed torque may be expressed in terms of rotor and stator flux:

$$T_e = \frac{M}{L_s \cdot L_r - M^2} \cdot \left|\vec{\psi}_s\right| \cdot \left|\vec{\psi}_r\right| \cdot \sin(\delta_\psi) \tag{15}$$

where δ_Ψ is the angle between the stator and the rotor flux linkage space phasors. For constant stator and rotor flux, the angle δ_Ψ may be used to control the torque of the motor. For a stator fixed reference frame ($\omega_e = 0$) and $R_s = 0$ it may be obtained that:

$$\psi_s = \frac{1}{T_n} \int_0^t u_s \cdot dt \tag{16}$$

The stator voltage space phasor may assume only six different non zero states and two zero states, as shown in Fig. 16. The change of the stator flux vector per switching instant is therefore determined by equation (16) and Fig. 16. The zero vectors V_0 and V_7 halt the rotation of the stator flux vector and slightly decrease its magnitude. The rotor flux vector, however, continues to rotate with almost synchronous frequency, and thus the angle δ_Ψ changes and the torque changes accordingly as per (15). The complex stator flux plane may be divided into six sections and a suitable set of switching vectors identified as shown in Table 1, where $d\Psi$ and dT_e are stator flux and torque errors, respectively, while $S_{1,\ldots,6}$ are sectors of 60° where stator flux resides.

Further researches in the field of DTC are mostly based on reducing torque ripples and improvement of estimation process. This yields to development of sophisticated control algorithms, constant switching schemes based on space-vector modulation (Casadei et al., 2003), hysteresis controllers with adaptive bandwidth, PI or fuzzy controllers instead of hysteresis comparators, just to name a few.

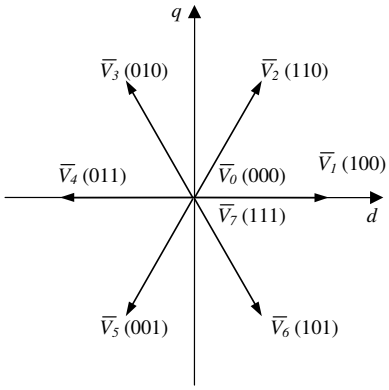

Fig. 16. Voltage vectors of three phase VSI inverter

dΨ	dT_e	S_1 $-\pi/6$, $\pi/6$	S_2 $\pi/6$, $\pi/2$	S_3 $\pi/2$, $2\pi/3$	S_4 $2\pi/3$, $-2\pi/3$	S_5 $-2\pi/3$, $-\pi/2$	S_6 $-\pi/2$, $-\pi/6$
1	1	V_2	V_3	V_4	V_5	V_6	V_1
	0	V_0	V_7	V_0	V_7	V_0	V_7
	-1	V_6	V_1	V_2	V_3	V_4	V_5
0	1	V_3	V_4	V_5	V_6	V_1	V_2
	0	V_7	V_0	V_7	V_0	V_7	V_0
	-1	V_5	V_6	V_1	V_2	V_3	V_4

Table 1. Optimal switching vectors in VSI DTC drive

4.2 Standard DTC of CSI drives

Although the traditional DTC is developed for VSI, for synchronous motor drives the CSI is proposed (Vas, 1998; Boldea, 2000). This type of converter can be also applied to DTC induction motor drive (Vas, 1998), and in the chapter such an arrangement is presented. The induction motor drives with thyristor type CSI (also known as auto sequentially commutated inverter) possess some advantages over voltage-source inverter drive. CSI permits easy power regeneration to the supply network under the breaking conditions, what is favorable in large-power induction motor drives. In traction applications bipolar thyristor structure is replaced with gate turn-off thyristor (GTO). Nowadays, current source inverters are popular in medium-voltage applications (Wu, 2006), where symmetric gate-commutated thyristor (SGCT) is utilized as a new switching device (Zargari et al., 2001) with advantages in PWM-CSI drives.

DTC of a CSI-fed induction motor involves the direct control of the rotor flux linkage and the electromagnetic torque by applying the optimum current switching vectors. Furthermore, it is possible to control directly the modulus of the rotor flux linkage space vector through the rectifier voltage and the electromagnetic torque by the supply frequency of CSI. Basic CSI DTC strategy (Vas, 1998) is shown in Fig. 17.

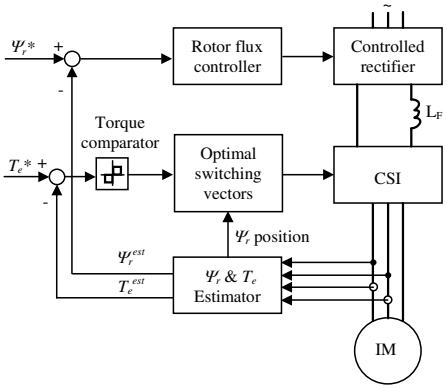

Fig. 17. DTC of CSI drive based on hysteresis control

The stator flux value, needed for DTC control loop, is not convenient to measure directly. Instead of that, the motor flux estimation is performed. In the voltage-based estimation method, the motor flux can be obtained by integrating its back electromotive force (EMF). The EMF is calculated from the motor voltage and current (17) and the only motor parameter required is the stator winding resistance. In practice, this simple integration is replaced by more sophisticated closed-loop estimators using filtering techniques, adaptive integration or even observers and Extended Kalman filters (Holtz, 2003).

$$\overline{\psi}_s^s = \int_0^t \left(\overline{u}_s^s - R_s \cdot \overline{i}_s^s \right) dt + \overline{\psi}_{s0}^s \tag{17}$$

For DTC of CSI fed induction motor drive, the appropriate optimal inverter current-switching vectors (Fig. 18) are produced by using an optimal current-switching table similarly to the table given for VSI drive (Table 2). The main difference is that in CSI exist only one hysteresis comparator for torque and only one zero switching current vector.

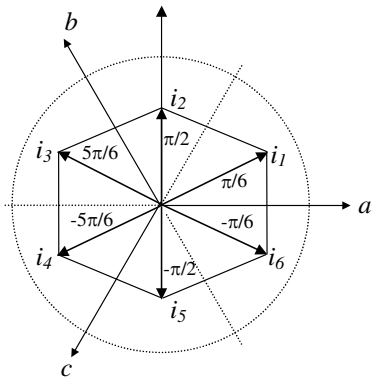

Fig. 18. Current vectors in CSI

dT_e	S_1 0, $\pi/3$	S_2 $\pi/3$, $2\pi/3$	S_3 $2\pi/3$, π	S_4 $-\pi$, $-2\pi/3$	S_5 $-2\pi/3$, $-\pi/3$	S_6 $-\pi/3$, 0
1	i_2	i_3	i_4	i_5	i_6	i_1
0	i_0	i_0	i_0	i_0	i_0	i_0
-1	i_6	i_1	i_2	i_3	i_4	i_5

Table 2. Optimal switching vectors in CSI DTC drive

4.3 Proposed DTC of CSI drives

In DTC schemes, the presence of hysteresis controllers for flux and torque determines variable-switching-frequency operation for the inverter. Furthermore, using DTC schemes a fast torque response over a wide speed range can be achieved only using different switching tables at low and high speed. The problem of variable switching frequency can be overcome by different methods (Vas, 1998; Casadei et al., 2003). In (Casadei et al., 2003), a solution based on a stator flux vector control (SFVC) scheme has been proposed. This scheme may be considered as a development of the basic DTC scheme with the aim of improving the drive performance. The input commands are the torque and the rotor flux, whereas the control variables are the stator flux components. The principle of operation is based on driving the stator flux vector toward the corresponding reference vector defined by the input commands. This action is carried out by the space-vector modulation (SVM) technique, which applies a suitable voltage vector to the machine in order to compensate the stator flux vector error. In this way it is possible to operate the induction motor drive with a constant switching frequency.

In proposed DTC CSI drive shown in Fig. 19 the inputs are rotor flux and torque as in VSI presented in (Casadei et al., 2003), but now as a control variable the stator flux angle α_s is used (Nikolic & Jeftenic, 2008).

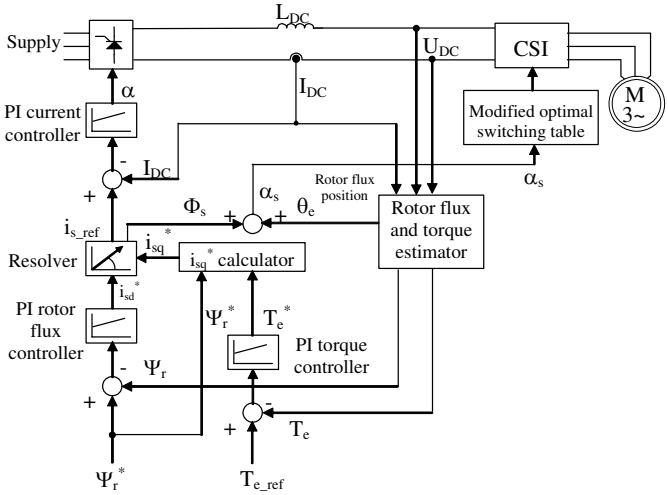

Fig. 19. Proposed constant-switching DTC strategy in CSI fed induction motor drive

Although this configuration could remind on field-oriented control, the main difference is absence of coordinate transformation since it is not necessary to use coordinate transformation to achieve correct firing angle as in vector control of the same drive (Nikolic & Jeftenic, 2006). Identical result would be obtained when phase angle Φ_s between d-q current references and rotor flux vector angle $\theta_e = \arctan(\Psi_{r\beta}/\Psi_{r\alpha})$ are summed and resulting angle α_s is than used to determine sector of 60 degrees where resides rotor flux vector. In that way, phase angle Φ_s acts as a torque control command. When reference torque is changed, i_{sq}* is momentary changed. Phase angle Φ_s "moves" stator current vector i_s in direction determined by the sign of torque reference and its value accelerate or decelerate flux vector movement according to the value of the reference torque (Fig. 20).

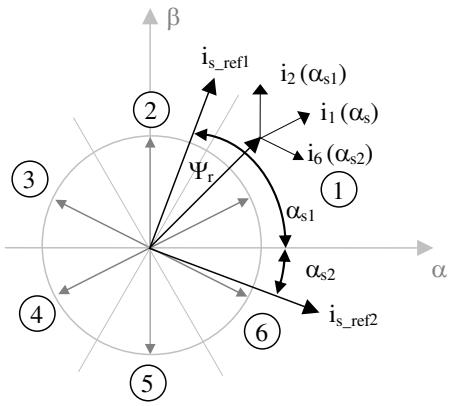

Fig. 20. Selecting proper current vector in proposed DTC algorithm

This modification implies somewhere different switching table for activating inverter switches from that shown in Table 2. Now α_s (angle between referent α-axis and reference current vector i_s) determines which current vector should be chosen: i_2 for torque increase, i_6 for torque decrease or i_1 for keeping torque at the current value.

Current vector	Angle range (degrees)
i_1	$\alpha_s > 0°$ and $\alpha_s \leq 60°$
i_2	$\alpha_s > 60°$ and $\alpha_s \leq 120°$
i_3	$\alpha_s > 120°$ and $\alpha_s \leq 180°$
i_4	$\alpha_s > 180°$ or $\alpha_s \leq -120°$
i_5	$\alpha_s > -120°$ and $\alpha_s \leq -60°$
i_6	$\alpha_s > -60°$ and $\alpha_s \leq 0°$

Table 3. Optimal switching table in proposed DTC

It is necessary to emphasize the importance of zero space vectors. In VSI there are two zero voltage vectors: V_0 denotes case when all three switches from the one half of inverter are switched ON while V_7 represent state when switches are OFF. Contrary, in CSI (using analogy to the VSI) zero current vector i_0 represent case when all thyristors are OFF. That could lead to both torque and motor speed decrease. Due to the nature of commutation in CSI, it is convenient to keep the selected current vector at instants when zero current vector is chosen.

The voltage and the current of CSI fed induction motor, necessary for stator flux calculation, can be reconstructed from the DC link quantities knowing the states of the conducting inverter switches. In one duty cycle of the output current CSI has six commutations. In that case six intervals of 60 degrees can be defined in which the current and the voltage changes its values. In every interval the current from DC link flows through two inverter legs and two motor phase windings. The motor line voltage is equal to the DC voltage on the inverter input reduced for the voltage drop on the active semiconductors, i.e. serial connection of the thyristor and diode in each inverter leg (Fig. 1). This voltage drop is forward voltage and for diodes it is about 0.7V-0.8V and for thyristors it is about 1V-1.5V. In this algorithm the average value of the overall forward voltage is used (2V), but for the practical realization it is chosen from the semiconductors datasheets or determined experimentally. It can be generally concluded that the voltage drop on the corresponding thyristor-diode par could have the following values in dependence of the conducting thyristor T_x, where x = 1,…,6:

- $V_{TDx} = V_F$, when T_x is conducting,
- $V_{TDx} = 0.5 \cdot U_{DC}$, when conducts thyristor from the same half-bridge where T_x is,
- $V_{TDx} = U_{DC} - V_F$, when conducts thyristor from the same inverter leg where T_x is.

These results are used for the voltage calculation in all conducting intervals, and they are summarized in Table 4. Prior to the flux estimation, the currents and voltages given in the Table 4 should be converted to α-β stationary frame.

The resistance of the stator windings, needed for stator flux calculation, can be easily determined from the simple experiment when the motor is in the standstill. When only thyristors T_1 and T_6 conducts, the DC current will flow through motor phases a and b. Since the motor is in the standstill, the only voltage drop is on the stator resistance R_s:

$$U_{ab} = 2 \cdot R_s \cdot i_a \tag{18}$$

when the windings are Y-connected. Generally, for the motor voltage value calculated from Table 4 and any type of the motor winding connection, the stator resistance is:

$$R_s = \frac{U_{ab}}{k_s \cdot i_a} = \frac{U_{DC} - 2 \cdot V_F}{k_s \cdot I_{DC}} \tag{19}$$

where k_s = 1 for Delta connection and k_s =2 for Y connection. Relation (19) can be easily implemented in the control software if the thyristors T_1 and T_6 are switched ON prior the motor start and the stator resistance is determined from the measured DC link current and voltage and the knowing voltage drop on the thyristor-diode par using Table 4.

	Active Thyristors	i_a	i_b	U_{ab}	U_{bc}
1	T1,T6	I_{DC}	0	$U_{DC} - 2 \cdot V_F$	$-0.5 \cdot U_{DC} + V_F$
2	T1,T2	I_{DC}	$-I_{DC}$	$0.5 \cdot U_{DC} - V_F$	$0.5 \cdot U_{DC} - V_F$
3	T3,T2	0	$-I_{DC}$	$-0.5 \cdot U_{DC} + V_F$	$U_{DC} - 2 \cdot V_F$
4	T3,T4	$-I_{DC}$	0	$-U_{DC} + 2 \cdot V_F$	$0.5 \cdot U_{DC} - V_F$
5	T5,T4	$-I_{DC}$	I_{DC}	$-0.5 \cdot U_{DC} + V_F$	$-0.5 \cdot U_{DC} + V_F$
6	T5,T6	0	I_{DC}	$0.5 \cdot U_{DC} - V_F$	$-U_{DC} + 2 \cdot V_F$

Table 4. Motor current and voltage determined only by DC link measurements

The main feedback signals in DTC algorithm are the estimated flux and torque. They are obtained as outputs of the estimator operating in stator reference frame. This estimator at first performs electro-motive force (EMF) integration (17) to determine the stator flux vector and than calculates the flux amplitude and find the sector of 60 degrees in α-β plane where flux vector resides, according to the partition shown in Fig. 20. After the stator current and voltage are determined by previously explained reconstruction of stator voltages and currents, pure integrator in (17) yields flux vector, which components are subsequently limited in amplitude to the magnitude values of the stator flux references. The trajectory of flux vector is not circular in the presence of DC offset. Since its undisturbed radius equals Ψ_s^*, the offset components tend to drive the entire trajectory toward one of the $\pm\Psi_s^*$ boundaries. A contribution to the EMF offset vector can be estimated from the displacement of the flux trajectory (Holtz, 2003), as:

$$EMF_{\alpha\beta}^{off} = \frac{1}{\Delta t} \cdot \left(\Psi_{\alpha\beta_{\max}} + \Psi_{\alpha\beta_{\min}} \right) \tag{20}$$

where the maximum and minimum values in (20) are those of the respective components $\Psi_{s\alpha}$ and $\Psi_{s\beta}$, and Δt is the time difference that defines a fundamental period. The signal EMF_{off} is fed back to the input of the integrator so as to cancel the offset component in EMF. The input of the integrator then tends toward zero in a quasi-steady state, which makes the estimated offset voltage vector equal the existing offset Ψ_{s0} in (17). The trajectory of Ψ_s is now exactly circular, which ensures a precise tracking of the EMF offset vector. Since offset drift is mainly a thermal effect that changes the DC offset very slowly, the response time of the offset estimator is not at all critical. It is important to note that the dynamics of stator flux estimation do not depend on the response of the offset estimator (Holtz, 2003).
The estimated rotor flux is calculated from the stator flux estimate using motor parameters and reconstructed stator current:

$$\hat{\Psi}_{r\alpha\beta} = \frac{L_r}{L_m} \cdot \hat{\Psi}_{s\alpha\beta} - \frac{L_s \cdot L_r - L_m^2}{L_m} \cdot i_{s\alpha\beta} \tag{21}$$

and its position in α-β reference frame is determined by:

$$\theta_e = \arctan\left(\frac{\Psi_{r\beta}}{\Psi_{r\alpha}} \right) \tag{22}$$

Finally, from the estimated stator flux and reconstructed current vector the motor torque is:

$$T_e = \frac{3}{2} p \cdot \left(i_{s\beta} \Psi_{s\alpha} - i_{s\alpha} \Psi_{s\beta} \right) \tag{23}$$

where the stator flux and current vectors are given in stationary α-β frame, and p denotes the number of poles.
The simulation model is developed in Matlab/SIMULINK, using SimPowerSystems block library that allows a very real representation of the power section (rectifier, DC link, inverter and induction motor). All electrical parameters (inductance of DC link, motor parameters) are the same as in real laboratory prototype, also used for testing previosly explained FOC algorithm. Rated flux is 0.8Wb and rated torque is 14Nm. Rectifier reference current is limited to 12A and reference torque is limited to 150% of rated torque (20Nm).

Comparison between the basic and proposed DTC of CSI induction motor drive are shown in Fig. 21, using the same mathematical model of CSI drive as used for FOC algorithm. Proposed DTC shows much better torque response from motor standstill.

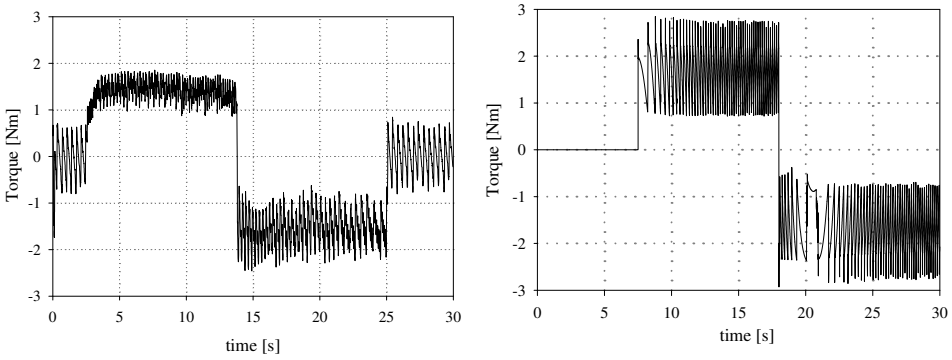

Fig. 21. Torque response for basic (left) and proposed (right) DTC algorithm

Dynamical performances of DTC algorithm are analyzed at first with rated flux and zero torque reference, than drive is accelerated up to 1000rpm. The speed is controlled in closed-loop via digital PI controller (proportional gain: $K_P = 5$, integral gain: $K_I = 0.5$, torque limit = 20Nm, controller sampling time: Ts = 4ms). The speed reference is set using succeeding scheme: +1000rpm at t = 0.25s, than –1000rpm at t = 0.6s. As could be seen from Fig. 22, a fast torque response is achieved with correct torque reference tracking and slow rotor flux ripple around the reference value (<1.5%).
For experimental purposes, the same laboratory prototype of CSI drive is used as explained before. The CSI feeds a 4kW induction motor and, as a mechanical load, the 6kW DC machine with controlled armature current is used (Nikolic & Jeftenic, 2008). The presented algorithm is not dependent on the motor power or the type of switching devices and it could be applied to any current source converter topology. The low-power induction motor and standard type thyristors are used just for the simplicity of the laboratory tests.
The torque response is analyzed both with direct torque demand and under the closed-loop speed control. Speed controller is implemented with soft start on its input and sample time of 20ms. Torque limit on the controller output is ±5Nm and is determined in such a way that under the maximum torque value slip is equal to maximal slip for current control:

$$s_{max} = \frac{1}{\omega_e \cdot T_r} = 0{,}0405 \tag{24}$$

where ω_e is synchronous frequency (314rad/s) and T_r is rotor time constant (78.7ms).
Since rotor flux is not measured but determined by estimation, its value is checked with that obtained from simulation. The comparison between simulated and estimated rotor flux whith zero speed (torque) reference and rated flux reference are given in Fig. 23 (a). Good performance of the flux estimator, necessary for proper direct torque control, could be observed from Fig. 23 (b), where flux trajectory is shown starting from zero to its rated value. Almost circular flux trajectory with equal amplitudes in both α and β axes assures correct offset compensation.

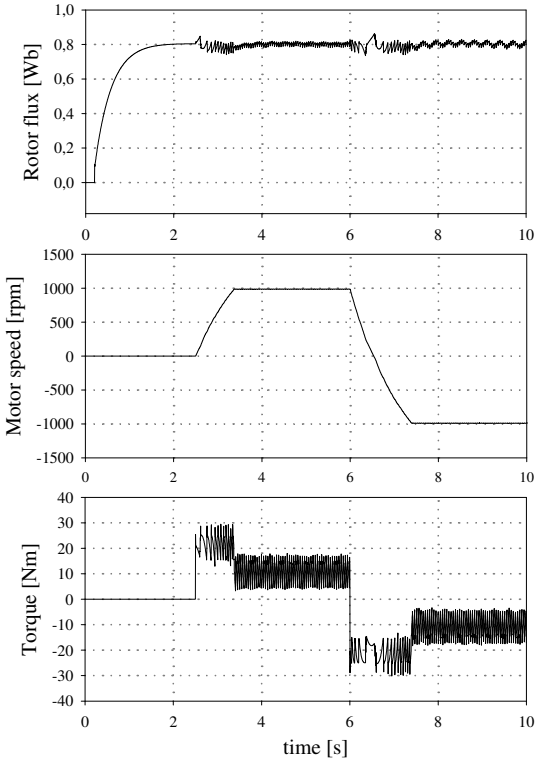

Fig. 22. Simulation results for the proposed DTC method

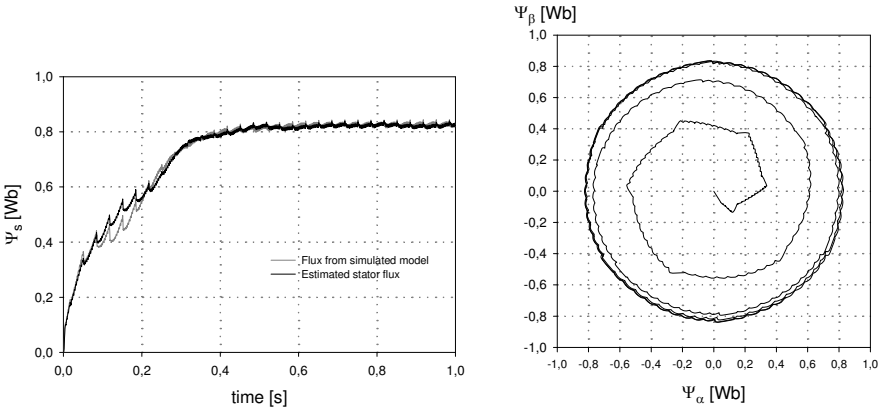

(a) (b)

Fig. 23. Rotor flux response (a) and its trajectory (b) during motor start-up

Motor speed and torque response when the speed control loop is closed is shown in Fig. 24. Response tests are performed during motor accelerating from 0rpm to 300rpm, than from 300rpm to 500rpm and back to 300rpm and 0rpm.

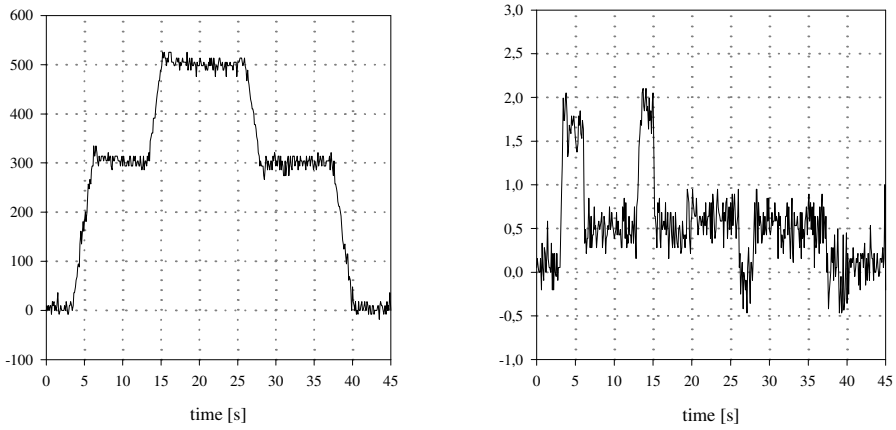

(a) (b)

Fig. 24. Motor speed (a) and torque (b) response under different speed references

5. Conclusions

In this chapter two main torque control algorithms used in CSI fed induction motor drives are presented, namely FOC and DTC. The first one is precise vector control (FOC) algorithm. The explained inconveniences of the vector controlled induction motor drives fed by a CSI could be overcome with the new vector control algorithm. The main advantage of the suggested algorithm compared to that known from the literature is better dynamic performances of the proposed CSI drive. This enhancement relies on the fast changes of the motor current, without phase error, similar to the control of current regulated voltage source PWM inverter. The realized CSI drive has more precise control, accomplished by the implemented correction of the reference current. This correction reduces the problem of the incorrect motor d-q currents values produced by the non-sinusoidal CSI current waveform.
Next, the two different methods of direct torque control in CSI fed induction motor drive are presented. Contrary to the well-known hysteresis control derived from VSI drive, new DTC algorithm based on the constant switching frequency is proposed. Merit of such a solution in comparison to the vector control of the same drive is absence of coordinate transformation and speed sensor on the motor shaft. Furthermore, since flux estimator is based only on DC link measurements, there is not necessity for any sensor on the motor side which is one of main drive advantages. In this case, by combination of vector control and basic DTC, a robust algorithm is developed that has a faster torque response and it is simpler for implementation. Moreover, algorithm is less sensitive to the parameter variation than standard FOC on the same drive. Contrary to the slip calculation using rotor time constant, proposed algorithm uses stator resistance for flux calculation and its value could be checked every time when motor is stopped using explained method for reconstruction

based only on DC link measurements. Other motor parameters (windings and mutual inductances) are used only when flux reference is changed and their values have no influence on the performance of the flux estimator due to the offset compensation. The validity of all presented torque control algorithms was proven by simulations and experimental results on developed laboratory prototype of CSI drive.

6. References

Blaschke, F. (1971). A new method for the structural decoupling of A.C. induction machines, *Proceedings of IFAC Symposium on Multivariable Technical Control Systems*, pp. 1–15, ISBN 0720420555, Duesseldorf, Germany, October 1971, American Elsevier, New York

Bose, BK. (1986). *Power Electronics and AC Drives,* Prentice-Hall, ISBN 0-13-686882-7, New Jersey, USA

Novotny, DW & Lipo, TA. (1996). *Vector Control and Dynamics of AC Drives*, Oxford University Press, ISBN 978-0-19-856439-3, New York, USA

B, Wu; SB, Dewan & Sen PC. (1988). A Modified Current-Source Inverter (MCSI) for a Multiple Induction Motor Drive System. *IEEE Transactions on Power Electronics,* Vol. 3, No. 1, January 1988, pp. 10-16, ISSN 0885-8993

Lorenz, RD. (1986). Tuning of Field-Oriented Induction Motor Controllers for High-Performance Applications, *IEEE Transactions on Industry Applications,* Vol. IA-22, No. 2, March 1986, pp. 293-297, ISSN 0093-9994

Deng, D & Lipo, TA. (1990). A Modified Control Method for Fast Response Current Source Inverter Drives, *IEEE Transactions on Industry Applications*, Vol. IA-22, No. 4, July 1986, pp. 653-665, ISSN 0093-9994

Vas, P. (1990). *Vector Control of AC Machines*, Clarendon Press, ISBN-10: 0198593708, ISBN-13: 978-0198593706, Oxford, New York, USA

Cavallini, A.; Loggini, M. & Montanari, GC. (1994). Comparison of Approximate Methods for Estimate Harmonic Currents Injected by AC/DC Converters, *IEEE Transactions on Industial Electronics,* Vol. 41, No. 2, April 1994, pp. 256-262, ISSN 0278-0046

Nikolic, A. & Jeftenic, B. (2006). Precise Vector Control of CSI Fed Induction Motor Drive, *European Transactions on Electrical Power*, Vol.16, March 2006, pp. 175-188, ISSN 0170-1703

Zargari, N. R.; Rizzo, S. C.; Xiao, Y.; Iwamoto, H.; Satoh, K. & Donlon, J. F. (2001). A new current-source converter using a symmetric gate-commutated thyristor (SGCT), *IEEE Transactions on Industry Applications*, Vol.37, 2001, pp. 896-903, ISSN 0093-9994

Takahashi, I. & Noguchi, T. (1986). A New Quick-Response and High-Efficiency Control Strategy of an Induction Motor, *IEEE Transactions on Industry Applications*, Vol. 22, No. 5, September/October 1986, pp. 820-827, ISSN 0093-9994

Depenbrok, M. (1988)., Direct Self-Control (DSC) of Inverter-Fed Induction Machine, *IEEE Transactions on Power Electronics*, Vol. PE-3, No. 4, October 1988, pp. 420-429, ISSN 0885-8993

Tiitinen, P.; Pohjalainen, P.& Lalu, J. (1995). The next generation motor control method: Direct Torque Control (DTC), *European Power Electronics Journal*, Vol.5, March 1995, pp. 14-18, ISSN 09398368

Buja, G.; Casadei, D. & Serra, G. (1998). Direct Stator Flux and Torque Control of an Induction Motor: Theoretical Analysis and Experimental Results, in *Proceedings of the IEEE International Conference on Industrial Electronics IECON '98*, pp. T50-T64, Vol. 1, ISBN 0-7803-4503-7, Aachen, Germany, August/September 1998, IEEE, New Jersey

Vas, P. (1998). *Sensorless Vector and Direct Torque Control*, Oxford University Press, ISBN 0-19-856465-1, New York, USA

Boldea, I. (2000). Direct Torque and Flux (DTFC) of A.C. Drives: A Review. *Proceedings of the 9th Conference EPE-PEMC 2000*, pp. 88-97, ISBN 80-88922-18-6, Kosice, Slovakia, September 2000, EPE-PEMC, Budapest

Casadei, D.; Serra, G.; Tani, A.; Zarri, L. & Profumo, F. (2003). Performance Analysis of a Speed-Sensorless Induction Motor Drive Based on a Constant-Switching-Frequency DTC Scheme, *IEEE Transactions on Industry Applications*, Vol.39, 2003, pp. 476-484, ISSN 0093-9994

Wu, B. (2006). *High-power converters and AC drives*, John Wiley & Sons, Inc., Hoboken, ISBN-13 978-0-471-73171-9, ISBN-10 0-471-73171-4, New Jersey, USA

Nikolic, A. & Jeftenic, B. (2008). Different Methods for Direct Torque Control of Induction Motor Fed From Current Source Inverter, *WSEAS Transactions on Circuits and Systems*, Volume 7, Issue 7, January 2008, pp. 738-748, ISSN 1109-2734

Holtz, J. (2003). Drift- and Parameter-Compensated Flux Estimator for Persistent Zero-Stator-Frequency Operation of Sensorless-Controlled Induction Motors, *IEEE Transactions on Industrial Applications*, Vol.39, 2003, pp. 1052-1060, ISSN 0093-9994

Torque Control

Edited by Prof. Moulay Tahar Lamchich

ISBN 978-953-307-428-3
Hard cover, 292 pages
Publisher InTech
Published online 10, February, 2011
Published in print edition February, 2011

This book is the result of inspirations and contributions from many researchers, a collection of 9 works, which are, in majority, focalised around the Direct Torque Control and may be comprised of three sections: different techniques for the control of asynchronous motors and double feed or double star induction machines, oriented approach of recent developments relating to the control of the Permanent Magnet Synchronous Motors, and special controller design and torque control of switched reluctance machine.

How to reference

In order to correctly reference this scholarly work, feel free to copy and paste the following:

Aleksandar Nikolic (2011). Torque Control of CSI Fed Induction Motor Drives, Torque Control, Prof. Moulay Tahar Lamchich (Ed.), ISBN: 978-953-307-428-3, InTech, Available from: http://www.intechopen.com/books/torque-control/torque-control-of-csi-fed-induction-motor-drives

INTECH
open science | open minds

InTech Europe
University Campus STeP Ri
Slavka Krautzeka 83/A
51000 Rijeka, Croatia
Phone: +385 (51) 770 447
Fax: +385 (51) 686 166
www.intechopen.com

InTech China
Unit 405, Office Block, Hotel Equatorial Shanghai
No.65, Yan An Road (West), Shanghai, 200040, China
中国上海市延安西路65号上海国际贵都大饭店办公楼405单元
Phone: +86-21-62489820
Fax: +86-21-62489821